AFGC-ACI-*fib*-RILEM Int. Symposium on Ultra-High Performance Fibre-Reinforced Concrete,
UHPFRC 2017 – October 2-4, 2017, Montpellier, France

EXPERIMENTAL STUDIES AND NUMERICAL ANALYSIS ON THE FLEXURAL BEHAVIOR OF REINFORCED UHPC BEAMS

Jia-zhan Su (1), Bao-chun Chen (1) and Qing-wei Huang (1)

(1) College of Civil Engineering, Fuzhou University, Fuzhou, China

Abstract

Application of ultra-high performance concrete (UHPC) in bridges has not been fully promoted due to the lack of the specification on bridge design using UHPC in China. A systemic research with an emphasis on experimental investigation and finite element analysis of UHPC beams is carried out in this study, focusing on the mechanical behavior, failure mode, crack resistance, and ultimate load carrying capacity. Total of 12 reinforced UHPC beams and 2 reinforced concrete (RC) beams are tested, taking steel fiber volume fraction and reinforcement ratio as the key parameters. Utilizing the general purpose program ABAQUS, the finite element model (FEM) for analyzing UHPC beam is established. The effect of different parameters on bending behaviors is investigated using FEMs, including steel fiber volume fraction, reinforcement ratio, yield strength of rebar, and compressive and tensile strength of UHPC. The calculation model is determined according to the mechanical behavior and failure mode of the reinforced UHPC beam.

Résumé

L'emploi du béton fibre à ultra-hautes performances (BFUP) dans les ponts n'a pas été pleinement promu en Chine à cause du manque de clauses concernant le calcul des ponts en BFUP. Une recherche systématique comprenant notamment des essais et une analyse aux éléments finis est menée sur des poutres en BFUP et se concentre sur le comportement du matériau, le mode de ruine, la résistance à la fissuration et la capacité portante. Au total 12 poutres en BFUP armé et 2 témoins en béton ont été testées, la teneur volumique en fibres et le taux de ferraillage étant les paramètres clés de l'étude. La modélisation aux éléments finis des poutres en BFUP a été réalisée à l'aide du code généraliste ABAQUS. L'effet des différents paramètres (pourcentage de fibres, taux de ferraillage, limite élastique des armatures, résistance du BFUP en compression et en traction) sur la réponse en flexion a été étudié. Le modèle simplifié pour le calcul peut ainsi être déterminé en fonction du comportement mécanique et du mode de ruine de la poutre en BFUP armé.

1. INTRODUCTION

Ultra-high performance concrete (UHPC) refers to a new type of cement-based composite material exhibiting ultra-high compressive strength, good tensile behaviour, high toughness, and excellent durability [1]. It has a broad application prospects in civil engineering, including bridges, buildings, nuclear engineering, municipal structures, ocean engineering, due to its different roles in reducing the structural self-weight, enhancing the bearing capacity, and improving the ductility [2-5]. Recommendations or design guide for UHPC were proposed in France, Switzerland, and USA [6-8]. In China, however, application of UHPC in bridges has not been fully promoted due to the lack of the specification on bridge design using UHPC. Therefore, in order to improve the relevant design/construction standards in China, investigation of UHPC beams using local materials is carried out in this study, focusing on the mechanical behaviour, failure mode, crack resistance, and ultimate load carrying capacity.

2. TEST SPECIMENS AND TEST SET-UP

In order to better understand the mechanical behaviour of UHPC beams, a static test with rather detailed measurements was conducted on 12 UHPC specimens and two reinforced concrete (RC) beams, taking steel fiber volume fraction and reinforcement ratio as the key parameters. All specimens were same in profiles with a cross section of 150 mm by 120 mm and a clear span of 1000 mm, as shown in Figure 1. The fiber content varied between 0 to 3% and the longitudinal reinforcement ratio was 0.8%, 1.8%, 3.8%. Table 1 lists the parameter of the specimens. The mixture proportion of UHPC with a water-to cementitious materials ratio of 0.18 a silica fume-to cementitious materials ratio of 0.3, and a sand-to cementitious materials ratio of 1.2 was used. The super-plasticizer was fixed at 2.5% by the mass of the cementitious materials. Steel fiber contents of 0, 1%, 2%, and 3% by the volume of concrete were used. All specimens were cured at 90℃ and relative humidity >95% for 72 hours after mould stripping. The cube compressive strength of UHPC on 100 mm × 100 mm × 100 mm and prism compressive strength on 100 mm × 100 mm × 300 mm at the age of 28 days, as well as the Young's elastic modulus were listed in Table 2. The flexural strength of test specimens subjected to a 4-point bending test on 100 mm × 100 mm × 400 mm were also listed in Table 2.

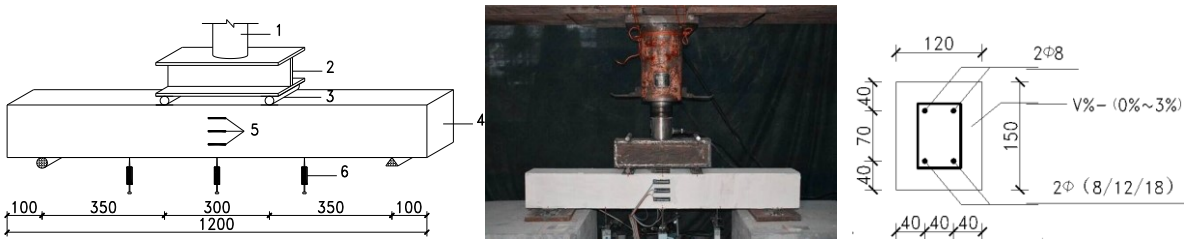

1-jack, 2-load-distribution beam, 3-block, 4-specimen, 5-strain gage, 6-LVDTs

Figure 1: Configuration of specimen (Unit: mm)

The beams were mounted on two stiffened steel pedestals. The main characteristics of the test set-up and fixtures are shown in Figure 1. The physical end supports allowed one end of the beam to move freely thus simulating the intended simply supported boundary conditions. The support also allowed the beams to rotate and the lateral supports prevented the beams from moving and rotation laterally. The specimens were loaded on a 1,000 kN capacity

testing machine. The loads were applied to the specimens as line loads across the top surface symmetrically at the two loading points.

Table 1: Parameter of specimens

No.	Type	Reinforcement	Reinforcement ratio	Fiber volume	Stirrup
L-1-1	UHPC	2Φ12mm	1.8%	2%	Φ6mm @150
L-1-2		2Φ8mm	0.8%	2%	
L-1-3		2Φ18mm	3.8%	2%	
L-2-1		2Φ12mm	1.8%	0%	
L-2-2		2Φ12mm	1.8%	1%	
L-2-3		2Φ12mm	1.8%	3%	
L-3-1	RC	2Φ12mm	1.8%	—	

Table 2: Material properties of UHPC

Fiber volume	Cube compressive strength（*MPa*）	Prism compressive strength (*MPa*)	Young's modulus (*GPa*)	Flexural strength (*MPa*)
0	104.67	85.94	35.15	15.90
1%	108.37	103.63	36.97	18.33
2%	118.63	114.16	38.72	20.47
3%	127.23	123.34	39.8	22.67

3. TEST PROCEDURE AND EXPERIMENTAL RESULTS

3.1 Test procedure and observations at failure

The cracking behaviour of UHPC beam was observed to be significantly different than would be expected in a conventional concrete beam. As shown in Figure 2, the extreme tensile fiber of this UHPC beam displayed a very high crack density. The crack spacing at any cross section along the span was observed to be inversely proportional to the maximum tensile strain experienced by the bottom fiber as a result of flexural forces applied to the beam.

Failure of the specimen was characterized by concrete yielding beginning at mid-span section, follow by the crush of the top surface in compression. The RC beam and the UHPC beam without steel fiber comes apart completely at their ultimate load, while the UHPC beams with steel fiber are still connected integrally even if they have many cracks at the ultimate load.

Figure 2: Failure model of specimen L-1-1

3.2 Detailed results

The measured load-deflection curves at the mid-span of UHPC beams and RC beam are shown in Figure 3(a). From these curves, three distinct phases were observed as elastic (linear), elastic-plastic, and plastic phase. It is obvious that high steel fiber volume increases the beam's rigidity and ductility. In the crack development stage, random distribution of steel fibers can effectively slow the crack development. The load-strain curves at mid-span section of specimens are plotted in Figure 3(b). The strain gages readings have a similar pattern in elastic range. With the increased steel fiber volume, the tensile strain in longitudinal steel bar near to the loading position decreased, which indicates that the steel fiber limits the tensile strain development of steel bar.

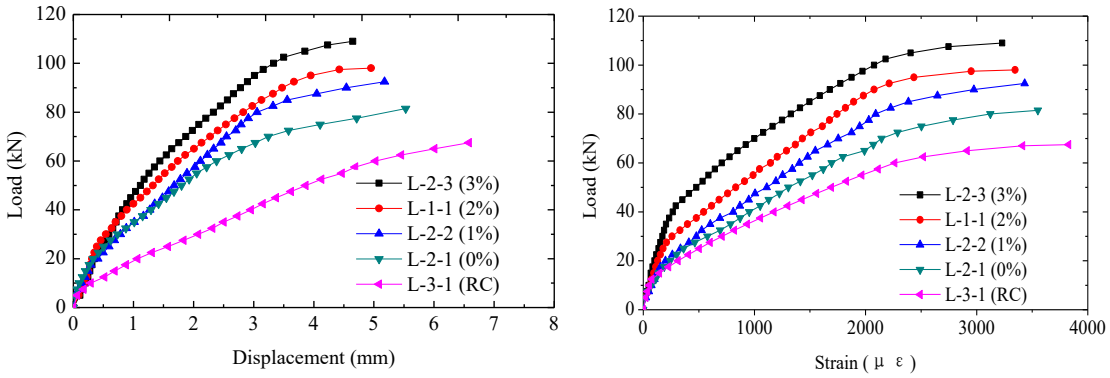

(a) Load-deflection curves (b) Load-strain curves

Figure 3: RC beam and UHPC beams with different steel fiber volume

Table 3 shows the comparison of the critical loads between different beams. The bending behaviour and failure mode of UHPC beam has three different stages of elastic stage, crack development stage, and failure stage, which is similar to that of RC beam. Compared with RC beam, the UHPC beams exhibit the capability of increasing the cracking load, yielding load, and failure load. Moreover, the increment is more and more with the increase of steel fiber volume. It is indicated that UHPC beam has a superior flexural behaviour than RC beam. The cross-sectional dimension of UHPC beam can be designed smaller than RC beam at the same design load. And thus the structural weight and construction difficulty can be reduced.

Table 3: Comparison of critical loads between RC beam and UHPC beams

Type	No.	Crack load (*kN*)	Yield load (*kN*)	Failure load (*kN*)
RC	L-3-1	12.5	60.0	67.5
UHPC	L-2-1（0% volume）	15.0	70.0	81.5
	L-2-2（1% volume）	17.5	80.0	92.5
	L-1-1（2% volume）	25.0	92.5	98.0
	L-2-3（3% volume）	35.0	102.5	109.0

The second parameter to be studied is the reinforcement ratio. This study was done by changing the diameter of steel bar. Three beams for each of specimen L-1-3, L-1-1 and L-1-2 were studied with reinforcement ratio of 0.8%, 1.8% and 3.8%. The load-deflection curves were plotted in Figure 4. It can be seen that with the increase of reinforcement ratio from 0.8% to 3.8%, the ultimate load was substantially increased. In addition, the elastic-plastic phases of the curves are longer and smoother for the beam has high reinforcement ratio.

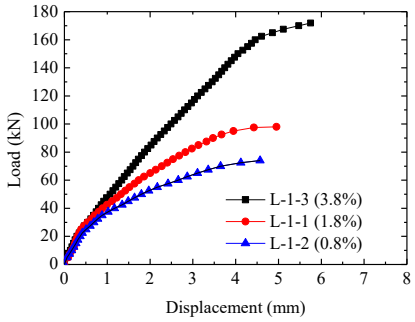

Figure 4: Load-deflection curves

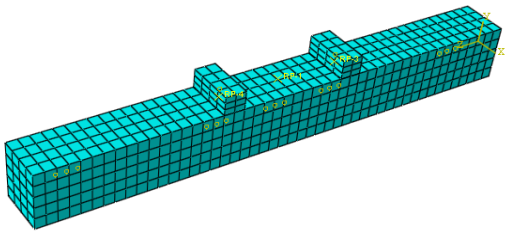

Figure 5: FE mesh of the beam

4. NUMERICAL ANALYSIS RESULTS

4.1 Finite element analysis results

For further studying of the flexural behaviour of UHPC beams, the finite element program, ABAQUS, is used for 3-D analyses of UHPC beams. The objectives of the analysis are to explain the discrepancies of experimental results, and to enhance the understanding of the accuracy of the theorectical assumptions for the problems. Throughout the studies, both the concrete and the loading blocks were modeled using solid element, C3D4, while truss element (T3D2) was used for the reinforcement. Figure 5 shows the FE mesh of a tested beam. The mesh was configured as 988 elements and 860 nodes. The boundary condition of the FE model was configured as close as possible to the boundary condition of the test. The loads were applied to the top loading blocks as concentrated loads at the test load points. To model the boudary conditions associated with the bottom surface, the transversal displacement DOF associated with the nodes at the supports were restrained.

The compressive constitutive relationship proposed by Du (2014) [9] was adopted for concrete in the FE analyses, as shown in Equation (1). The tensile constitutive relationship proposed by Du (2014) [9] was adopted, as shown in Equation (2).

$$y = \begin{cases} 1.2x - 0.2x^6 & (0 \le x \le 1) \\ \dfrac{x}{10(x-1)^2 + x} & (x \ge 1) \end{cases} \tag{1}$$

$$y = \begin{cases} \dfrac{x}{0.92x^{1.09} + 0.08} & 0 \le x < 1 \\ \dfrac{x}{0.1(x-1)^{2.4} + x} & 1 \le x \end{cases} \tag{2}$$

where: $x = \varepsilon / \varepsilon_p$ $\quad y = \sigma / f_c$ (3)

in which, ε and σ are the strain and stress at the intersecting point of the first portion and the second portion on the stress-strain curve of the UHPC; ε_p is the strain when the stress f_c of the concrete reaches its peak value.

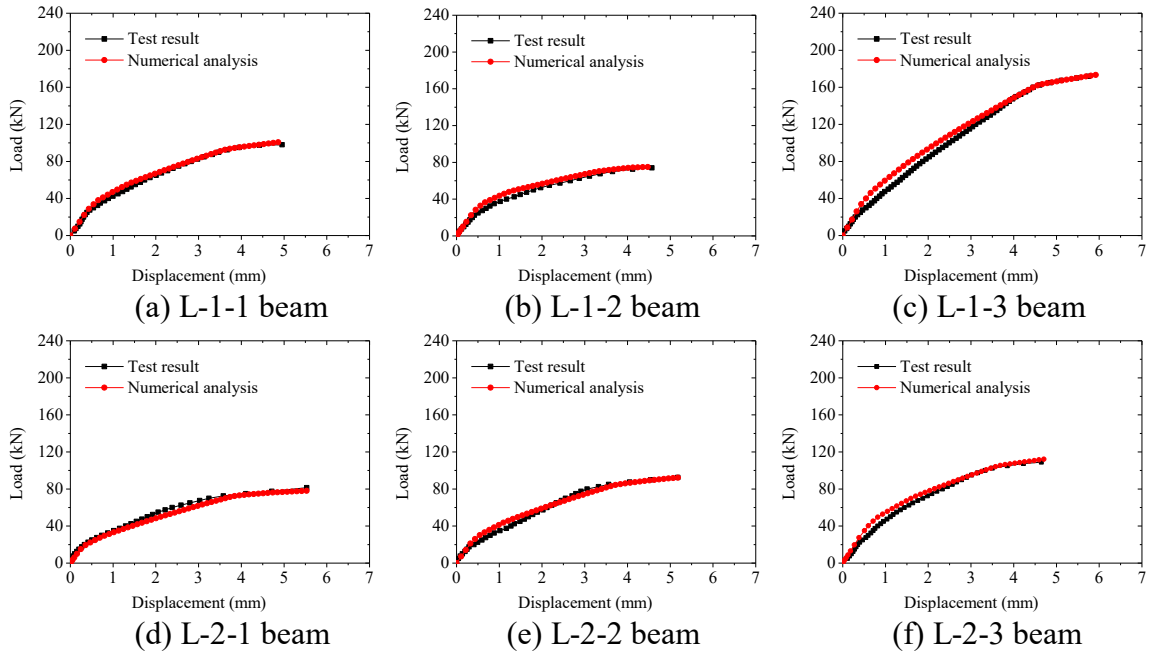

Figure 6: Load-deflection curve of beams

Table 4 Comparison between calculation results and test results

Specimen	Cracking load			Yield load			Failure load		
	Test result N_c (kN)	FE result N_c' (kN)	N_c/N_c'	Test result N_y (kN)	FE result N_y' (kN)	N_y/N_y'	Test result N_u (kN)	FE result N_u' (kN)	N_u/N_u'
L-1-1	25.00	26.85	0.87	92.50	92.68	1.00	98.00	100.67	0.97
L-1-2	22.50	22.55	1.00	70.00	71.75	0.98	74.00	74.93	0.99
L-1-3	27.50	25.98	1.06	160.00	162.05	0.99	171.90	173.41	0.99
L-2-1	15.00	15.10	0.99	70.00	71.28	0.98	81.50	77.03	1.06
L-2-2	17.50	19.22	0.82	80.00	81.52	0.98	92.50	96.22	0.96
L-2-3	35.00	37.37	0.87	102.50	102.44	1.00	109.00	112.13	0.97

It can be seen from Figure 6 that good agreement is achieved between the test result and the 3-D FE prediction. Table 4 lists the cracking load, yield load and failure load of both FEA and test of specimens. It can be noticed that values of N_c/N_c', N_y/N_y', and N_u/N_u' are very close to 1.000. Calculations showed that average values of N_c/N_c', N_y/N_y', and N_u/N_u' are all 0.97,

0.99, and 0.99, respectively, while the mean square deviation is 0.05, 0.01, 0.03, respectively. Figure 7 shows the crack distribution of the FE model. The red area is crack area, while the black lines are the cracks, which are basically matched with test result. Therefore the proposed numerical analysis approach can be employed to analyse well the mechanical behaviour of UHPC beams.

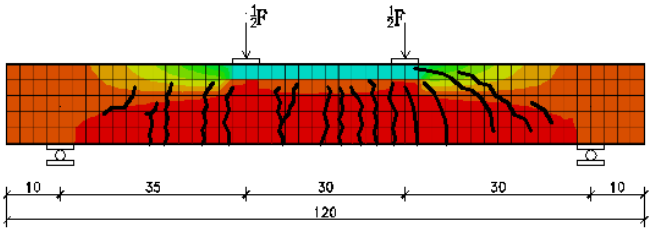

Figure 7: Crack distribution

4.2 Parametric studies

It has been shown in Section 4.1 that the FE model can be used to model the UHPC beams with excellent accuracy. Therefore, finite element based parametric studies are conducted to form a generalized equation to calculate the ultimate limit state of UHPC beams. A number of influencing parameters are identified such as steel fiber volume fraction, reinforcement ratio, yield strength of rebar, and compressive and tensile strength of UHPC. For each parameter study, a minimum of six values for each parameter are studied numerically. As the starting point for each study, the benchmark case is considered. The benchmark case is based primarily on the geometry, materials, and loading of the experimental tests, thus being directly verified against physical testing. With the benchmark configuration determined, different parameter variations are applied independently. The result indicates that the reinforcement ratio has great influence on the mechanical properties after cracking as well as yielding and failure loads of UHPC beams, while the steel fiber volume fraction has great influence on the mechanical properties in the elastic stage and its cracking load, as shown in Figure 8.

The yielding and failure loads increase linearly with the yield strength of rebar increases, and the ductility of UHPC beam could increase effectively. Besides, compressive strength of UHPC has less effect on the cracking and yielding loads than it does on failure load slightly, while tensile strength of UHPC has better effect on the cracking load than the yield and failure loads, as shown in Table 5.

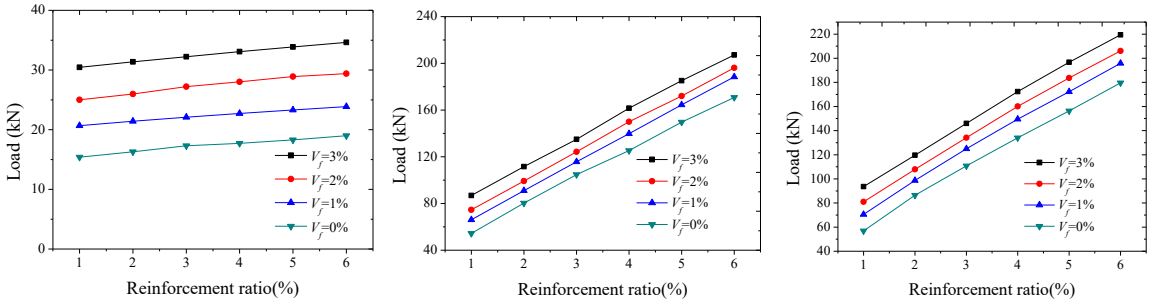

(a) Cracking load (b) Yield load (c) Failure load

Figure 8: Relationship between load and steel fiber volume fraction and reinforcement ratio

Table 5 List of calculation results

Concrete compressive strength (MPa)	Cracking load (kN)	Yield load (kN)	Failure load (kN)	Tensile strength of concrete (MPa)	Cracking load (kN)	Yield load (kN)	Failure load (kN)
100	32.38	152.73	161.06	6	16.19	135.81	144
125	32.38	153.21	168.91	8	24.29	145.48	153.24
150	32.38	153.01	173.57	10	32.38	152.73	161.06
175	32.38	153.17	177.43	12	40.47	163.99	168.44
200	32.38	153.1	180.26	14	48.55	172.17	175.39

4.3 Simplified calculation method for the ultimate load-carrying capacity

The distribution and simplified assumption of stress and strain of normal section subjected to bearing capacity are shown in Figure 9(a). It assumes the stress of concrete in the compressive zone as a triangle, while the stress in the tensile zone is equivalent to a rectangle. It is taken as the ultimate tensile strength f_t multiplied by a reduced factor K. Equations (4) and (5) can be obtained according to the equilibrium condition. A_s is the area of reinforcement; b and h are the width and height of the beam; a_s is the distance from reinforcement force to the beam bottom flange; ε_{cu} is ultimate compressive strain of UHPC beam; ε_t is the tension strain in tension zone when UHPC beam bearing ultimate force; σ_{cu} is limit compressive stress in compression part of concrete; f'_{rt} is bending strength; f_t is the ultimate tensile strength; K is strength reduction coefficient; x_c is the height of compression zone when bearing the limit force; x_t is the height of tension zone, $x_t=h-x_c$.

America FHWA [7] approximates the concrete compressive stress by a triangular stress distribution, and estimates the concrete tensile stress by a rectangle distribution, and the extreme value of tensile stress is the ultimate tensile strength, as shown in Figure 9(b). In Switzerland MCS-EPFL [8], the concrete tensile stress in elastic area is ignored (Figure 9(c)).

According to the numerical results, the reduction factor K is between 0.80~1.0, and the average reduction coefficient of each beam is 0.88, so the reduction factor K is 0.88. The Equation (6) of the ultimate bearing capacity of the rectangular UHPC beam can be obtained by substituting the reduction factor.

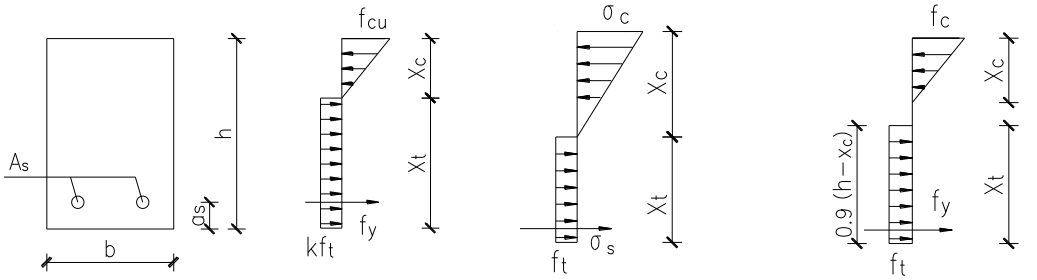

(a) Proposed by this study (b) FHWA [8] (c) MCS-EPFL [9]

Figure 9: Simplified assumption model of bearing capacity

$$\frac{1}{2} f_{cu} b x_c = k f_t b (h - x_c) + f_y A_s \tag{4}$$

$$M_u = \frac{1}{3} f_{cu} b x_c^2 + \frac{1}{2} k f_t b (h - x_c)^2 + f_y A_s (h - x_c - a_s) \tag{5}$$

$$M_u = \frac{1}{3} f_{cu} b x_c^2 + \frac{1}{2} \times 0.88 f_t b (h - x_c)^2 + f_y A_s (h - x_c - a_s) \tag{6}$$

Table 6 Finite element and calculation value of ultimate bearing capacity of UHPC beam (Unit: kN.m)

Beam No.	FE value	calculation value	Ratio	Beam No.	FE value	calculation value	Ratio
FEM-1	17.67	17.64	1.002	FEM-22	30.20	30.25	0.998
FEM-2	13.17	13.08	1.007	FEM-23	27.40	27.72	0.988
FEM-3	30.40	29.22	1.040	FEM-24	30.20	30.38	0.994
FEM-4	13.56	13.56	1.000	FEM-25	32.18	32.30	0.996
FEM-5	16.89	15.88	1.064	FEM-26	34.46	34.36	1.003
FEM-6	19.68	19.93	0.987	FEM-27	31.48	31.24	1.008
FEM-7	9.99	9.97	1.002	FEM-28	34.67	34.15	1.015
FEM-8	12.38	12.31	1.006	FEM-29	36.11	36.05	1.002
FEM-9	14.23	14.11	1.009	FEM-30	38.44	38.22	1.006
FEM-10	16.43	16.46	0.998	FEM-31	13.29	13.17	1.009
FEM-11	15.17	14.95	1.015	FEM-32	17.20	17.24	0.998
FEM-12	17.31	17.28	1.002	FEM-33	21.14	21.14	1.000
FEM-13	18.92	19.03	0.994	FEM-34	25.10	24.86	1.010
FEM-14	20.97	21.30	0.985	FEM-35	28.63	28.40	1.008
FEM-15	19.43	19.57	0.993	FEM-36	32.26	31.76	1.016
FEM-16	21.91	21.94	0.999	FEM-37	15.31	15.20	1.007
FEM-17	23.52	23.69	0.993	FEM-38	21.05	21.08	0.999
FEM-18	25.59	25.90	0.988	FEM-39	26.54	26.57	0.999
FEM-19	23.49	23.83	0.986	FEM-40	31.81	31.66	1.005
FEM-20	26.21	26.31	0.996	FEM-41	36.44	36.36	1.002
FEM-21	28.06	28.08	0.999	FEM-42	40.36	40.65	0.993

The calculation results using this method for the cases in this paper, including the test results and the FE results for parametric studies, are shown in Table 6, compared with the FEA results. This once again shows that the proposed method to calculate the ultimate load-carrying capacity of UHPC beams is effective. The average ratio between the calculations is only 1.003, and the square deviation is 0.014.

5. CONCLUSIONS

Experimental investigations on 12 UHPC beams and 2 RC beams are conducted, taking steel fiber volume fraction and reinforecement ratio as the key parameters. The simulated load-deflection curves, load-strain curves, and crack distribution are in agreement with the experimental results, which verify the effectiveness of the finite element analysis results. The reasonable calculation model is determined according to the mechanical behavior and failure mode of the UHPC beam. And then, the simplied calculation formula of cracking moment and flexural capacity is proposed based on the finite element anslysis results. It can be used as the reference in design and construction of similar structures in future.

ACKNOWLEDGEMENTS

This work is supported by the National Science Foundation under Grant No.U1305245, and Research Grant of the Fuzhou University (Project No. 510251) and the Education Department of Fujian Province (Project No. 601705).

REFERENCES

[1] Wang, D.H., Shi, C.J., Wu, Z.M., Xiao, J.F., Huang, Z.Y. and Fang, Z., 'A review on ultra-high performance concrete: Part II. Hydration, microstructure and properties', *Construction and Building Materials*. 96 (2015) 368-377.

[2] Chen, B.C., Šavor, Z., Su, J.Z. and Huang, Q.W., 'A state-of-the-art of ultra-high performance concrete arch bridges'.1st International Conference on UHPC Materials and Structures, Hunan University, (2016) 614-618.

[3] Russell, H.G. and Graybeal, B.A., 'Ultra-High Performance Concrete: A State-of-the-Art Report for Bridge Community', U.S. Federal Highway Administration. Publication No. FHWA-HRT-13-060 (2013).

[4] Voo, Y.L., Foster, S.J., Faiz, M. and Hassan, A., 'The current state of art of ultra-high performance concrete bridge construction in Malaysia'. Proceedings of the 12th International Conference on Concrete Engineering and Technology, 12-14 Aug., Selangor, Malaysia, (2014) 95-102.

[5] Voo, Y.L., Foster, S.J. and Voo, C.C., 'Ultra-high performance concrete segmental bridge technology: toward sustainable bridge construction', *Journal of Bridge Engineering, SPECIAL ISSUE: Design, Analysis, and Construction of Segmental Bridges*. B5014001. **20**(8) (2015).

[6] AFGC, Ultra high performance fibre-reinforced concrete. Recommendations, Revised Edition, Paris, 2013.

[7] U.S. Department of Transportation Federal Highway Administration (FHWA). Design Guide for Precast UHPC Waffle Deck Panel System, including Connections. FHWA-HIF-13-032, 2013.

[8] MCS-EPFL, Recommendation: Ultra-High Performance Fibre Reinforced Cement-based composites (UHPFRC), Construction material, dimensioning and application, Lausanne, Switzerland, 2016.

[9] Du, R.Y., 'Research on Ultimate Load-Carrying Capacities of Reactive Powder Concrete (RPC) Box Girder and Arch' Fuzhou University, (2014).